Nuclear Engineering and Design 447 (2026) 114647

Contents lists available at ScienceDirect

Nuclear Engineering and Design

journal homepage: www.elsevier.com/locate/nucengdes

Nickel-doped graphene films on stainless steel as efficient hydrogen recombination catalysts

L.M. Rios [a], L.De Micheli [a], G. Silvestrin [a], M. Durazzo [a], E.F. Urano de Carvalho [a], R.F.B. de Souza [b], C. Giovedi [a], E. Antolini [c], A.Oliveira Neto [a,*]

[a] Instituto de Pesquisas Energéticas e Nucleares, Cidade Universitária, 05508-000 São Paulo, SP, Brazil
[b] Comissão Nacional de Energia Nuclear, CNEN, Rio de Janeiro 22294-900 RJ, Brazil
[c] Scuola di Scienzadei Materiali, Via 25 Aprile 22, Cogoleto 16016 Genova, Italy

ARTICLE INFO

Keywords:
Passive autocatalytic recombiner (PAR)
Hydrogen oxidation
Graphene-coated stainless steel
Nickel catalyst

ABSTRACT

Nickel-doped catalysts supported on graphene-coated porous 304L stainless steel substrates were synthesized and evaluated for hydrogen recombination applications. The substrates, with a pore size of 50 μm, were doped with nickel loadings of 0.25, 0.50, 1.0, and 2.0 wt%. SEM analysis revealed that low nickel contents (0.25–0.50 wt%) resulted in a cracked, graphene-dominated surface and high BET surface area (up to 5.28 m^2/g for 0.5 wt% Ni), whereas higher loadings (1.0–2.0 wt%) promoted the formation of dispersed metallic and nickel particles, reducing the measured surface area. XRD patterns confirmed the coexistence of austenitic and martensitic phases, spinel-type oxides, graphene-related carbon phases, and nickel-containing phases (metallic Ni, NiO, Ni $(OH)_2$). Raman spectroscopy revealed a five-band model (D, G, D2, D3, D4), with characteristic modifications in defect density (decreasing ID/IG ratio) and distinct features near 500 cm^{-1} assigned to NiO, confirming the presence of metallic and oxidized nickel phases. No signals related to iron oxides or spurious nickel oxide were observed beyond these assignments. Water contact angle measurements demonstrated strong hydrophobicity (above 120°) for all samples, with a slight decrease at higher nickel loadings due to partial masking of graphene surfaces. Hydrogen recombination tests showed that catalytic performance improved with increasing nickel content, achieving approximately 63 % hydrogen removal with only 1.0 wt% Ni. The combined effects of high surface area (BET), well-dispersed nickel nanoparticles, and the graphene coating contributed to enhanced catalytic activity, efficient gas diffusion, and high surface hydrophobicity. These findings highlight nickel-based graphene-supported catalysts as an effective and economically viable alternative to platinum or palladium for hydrogen recombination in gas-phase applications.

1. Introduction

Hydrogen is widely recognized as a promising clean energy carrier due to its high gravimetric energy density and potential for zero-carbon emissions. Nevertheless, ensuring its safe handling remains a critical challenge, particularly in nuclear facilities where hydrogen may be generated during severe accident events. The accumulation of hydrogen in confined spaces poses severe explosion and fire hazards, underscoring the need for robust mitigation strategies to preserve structural integrity and operational safety. Among different solutions, Passive Autocatalytic Recombiners (PAR) are the most effective, which catalytically convert hydrogen and oxygen into water without requiring external energy input (Santos et al., 2020; Karimi et al., 2008). A PAR is a safety device based on the catalytic hydrogen combustion (CHC), i.e., on the exothermic reaction of H_2/O_2 on a catalytic material. The H_2/O_2 recombination occurs as the following reaction:

$$2H_2 + O_2 \rightarrow 2H_2O + 244.9 kJmol^{-1} \quad (1)$$

A PAR is a vertical flow channel, where incoming hydrogen from the bottom pass through the catalytic section and the products are removed from the top. A PAR is equipped with catalytic elements in the lower part, assembled into the catalytic block. The catalytic elements can have different shapes such as plate-type and cylindrical-type. Malakhov et al. (Malakhov et al., 2024) investigated the operational behavior of cylindrical-type catalysts used in a PAR by an experimental device and Computational Fluid Dynamics (CFD) analyses to evaluate the catalyst

* Corresponding author.
E-mail address: aolivei@usp.br (A.Oliveira Neto).

https://doi.org/10.1016/j.nucengdes.2025.114647
Received 1 September 2025; Received in revised form 18 November 2025; Accepted 1 December 2025
Available online 4 December 2025

temperature distribution and hydrogen conversion inside the PAR channel. Results showed that the catalyst has a fairly good conversion efficiency. Moreover, the temperature over the catalyst section is evenly distributed and it does not exceed the lower hydrogen ignition limit.

The main materials used in plate-type PAR are metallic plates coated with catalyst powder without an intermediate coating, and stainless steel plates coated with either a ceramic or a carbon-based layer, supporting a catalyst.

The reliable performance of PAR strongly depends on the selection of suitable structural and catalytic materials. Austenitic stainless steels, such as AISI 304L, are widely used in nuclear reactor components due to their excellent mechanical strength, corrosion resistance, and thermal stability under extreme conditions (Lee et al., 2021). The microstructural behavior of 304L stainless steel including phenomena such as martensitic transformations and oxide layer formation at elevated temperatures has been extensively characterized to predict durability in harsh environments (Shen et al., 2010). Structural parameters obtained from techniques like X-ray diffraction have also proven valuable in understanding activation and stability in carbon-based materials, including carbon black and graphene coatings (Simões et al., 2010).

In recent years, carbon-based materials such as graphene have attracted significant attention owing to their exceptional electrical conductivity, chemical inertness, and high surface area. When applied as a coating to metallic substrates, these properties can substantially enhance catalytic efficiency (Lu et al., 2021; Wu et al., 2018; Ferrari and Basko, 2013). The nature of the metal–carbon interaction is a decisive factor in determining catalytic performance; for example, studies on platinum–carbon coordination have shown a direct relationship between bonding characteristics and catalytic activity (Day et al., 1981). Furthermore, the presence and control of edge defects in graphene critically influence its electronic and catalytic behavior, as revealed by Raman spectroscopy analyses (Malard et al., 2009; Koyakutty et al., 2023; Ten et al., 2020).

Advances in this field have been driven by both materials science and nuclear safety research. For instance, De Micheli et al. (De Micheli et al., 2025) reported electrochemical characterizations that improved hydrogen oxidation kinetics and overall catalyst performance. Complementary reviews on nuclear plant safety emphasize emerging strategies for hydrogen risk mitigation and PAR optimization, highlighting the central role of advanced materials (Karoui et al., 2010; De Micheli et al., 2024). One promising approach involves doping graphene-coated stainless steel with transition metals such as nickel, offering a cost-effective alternative to precious metals like platinum or palladium while maintaining high catalytic activity and stability under oxidative conditions (Shen et al., 2010; Simões et al., 2010; Koyakutty et al., 2023).

Precious metals, like platinum and/or palladium, were used as catalysts for PAR. Sanap et al. (Sanap et al., 2015) prepared mixed Pt-Pd supported on stainless steel wire gauze and cordierite for the PAR. Both Pt–Pd/Wg and Pt–Pd/Cord were highly effective for hydrogen removal in 1.5 % to 7 % H_2 concentration in air. Both catalysts were poisoning tolerant *vs.* CO (up to 1200 ppm) and inhibitor like CO_2, CH_4 and relative humidity. The Pt–Pd/Cord catalyst showed higher CO tolerance and lower temperature rise for safer application at higher hydrogen concentrations than Pt–Pd/Wg. However, the stability of these catalysts was not evaluated. Indeed, an important issue of PAR catalysts is the low durability, due to Pt aggregation and catalyst support degradation, decreasing the catalytic activity. In this regard, some support can enough suppress precious metal sintering via a strong noble metal–support bond. For example, the bond energy between Pt and Al_2O_3 is relatively weak compared to the Ce–Zr–Y (CZY) mixed oxides. The annealing of Pt/Al_2O_3 catalyst at 800 °C for led to Pt aggregation, while no aggregation was observed for a Pt/CZY mixed oxide catalyst.

Catalytic hydrogen combustion (CHC) plays a key role in PARs. In a recent study, in their preliminary investigations, Kozhukhova et al. (Kozhukhova et al., 2021) used anodized aluminum oxide (AAO) as a Pt support for CHC purposes. The Pt/AAO catalyst showed high stability was over a prolonged CHC reaction time of 530 h. The AAO substrate has high thermal conductivity, preventing the formation of dangerous "hotspots" by dissipating heat, enhancing the stability of the Pt nanoparticles and the catalyst performance. The heat generated during CHC displaced from the AAO to the Al core, achieving a mild average catalyst surface temperature, which likely limited Pt aggregation. Thus, the utilization of the Pt/AAO catalyst in PAR can be a solution for low thermal conductive catalysts currently used in PARs. Then, they synthesized a Pt/CZY/AAO catalyst for CHC applications, combining the high thermal stability and the ability to stabilize Pt particles of Al/AAO and CZY supports, respectively (Kozhukhova et al., 2022). The Pt/CZY/AAO catalyst showed high catalytic activity and durability for the CHC at H_2concentrations of 1–8 vol%.A temperature of 454.1 °C was measured at 8 vol% H_2, considerably below the auto ignition temperature of hydrogen (585 °C), indicating that a PAR with a Pt/CZY/AAO catalyst can operate safely at concentrations >8 vol%.A maximum ΔT of 3.9 and 5.4 °C was observed at 3 vol% H_2. Moreover, a lower ΔT for the larger Pt/CZY/AAO catalytic plate the smaller catalyst was found, suggesting that the utilization of larger catalysts reduces the risk of hotspots occurrence. From these results, it can be inferred that the Pt/CZY/AAO catalyst has a great potential as a CHC catalyst for PAR application.

Open-cell metallic foams are promising candidates as PAR catalysts, due to their interconnected open cells, resulting in a low pressure drop and making easy gas transfer. Moreover, foams have an expanded surface area and increased reaction sites as catalyst support. Pt/Al_2O_3-coated Al foams were evaluated for the PAR (Kozhukhova et al., 2022). High H_2 conversions (57–89 %) were obtained and the catalyst activity was maintained for > 480 h on stream. Temperatures at the hottest spots on the foam surface reached a maximum of only 393 °C at the highest H_2 in flow. This work attests the effectiveness of a foam-supported catalyst for the PAR process. However, further studies are necessary to confirm the benefits of foam-supported catalysts for PAR applications. Nickel presents considerable catalytic activity across a diverse array of reactions. Zhang et al. (Musavuli et al., 2024) prepared pine needle-like Pt-Pd nano-dendrites catalysts by the impregnation method and the Pt-Pd/Ni foam nanosheet catalysts by the electrodeposition method. Both methods successfully integrated Pt and Pd into the Ni foam matrix with minimal changes in catalytic activity during prolonged use. Pt-Pd/Ni foam can achieve a 51.96 % H_2conversion rate at a flow rate of 0.05 m/s, with 4 vol% hydrogen and 21 vol% oxygen. Both impregnation and electrodeposition methods can be used to prepare Pt-Pd/Ni foam catalysts for PARs, resulting in catalysts with outstanding stability and heat dissipation.

The utilization of noble metals as CHC catalysts is limited by their high cost. Generally, non-noble metal catalysts display lower catalytic activity than noble metal catalysts. However, they possess the advantages of cost-effectiveness, superior thermal stability, and adequate activity under specific conditions. Among them, copper, nickel, perovskite-type compounds, spinel, and fluorite compound oxides showed notable activity in hydrogen catalytic combustion (Musavuli et al., 2024). The challenge is to develop non-noble metal catalysts with catalytic activity close to that of noble metal catalysts while improving cost efficiency.

These developments are consistent with the electrochemical insights and safety considerations reported in the literature (De Micheli et al., 2025; Karoui et al., 2010; De Micheli et al., 2024).Commercial PAR typically employ alumina spheres as catalyst supports. However, the use of stainless steel substrates offers a significant advantage in terms of superior heat dissipation, which can enhance thermal management and improve overall catalytic performance under operational conditions (De Micheli et al., 2024).

De Micheli (De Micheli et al., 2025) demonstrated that an optimized platinum loading of 0.5 wt% combined with a substrate porosity of 50 μm achieved a maximum hydrogen conversion efficiency of 40 %. However, the high cost of platinum and its indiscriminate use,

contributing to its depletion in the Earth's crust, leads to investigate more cheap and abundant elements, such Ni and Cu, which can provide comparable selectivity for the hydrogen oxidation reaction.

Despite significant technological progress, the optimization of catalyst composition, microstructure, and porosity remains a decisive factor for maximizing hydrogen conversion efficiency and ensuring the long-term operational reliability of PAR under severe accident conditions in Nuclear Power Plants (NPP).

This study focuses on the design and fabrication of catalytic substrates based on porous sintered 304L stainless steel coated with graphene and doped with nickel. The material combines the structural stability of stainless steel, the electrical conductivity of graphene, and the catalytic activity of nickel as a practical alternative to platinum. The objective is to develop and evaluate nickel-doped, graphene-coated stainless steel catalysts for hydrogen recombination, analyzing the influence of nickel loading and substrate structure on catalytic activity, gas diffusion, and surface hydrophobicity. The study also examines the relationship between physicochemical characteristics and hydrogen oxidation performance to support the development of efficient materials for hydrogen mitigation systems, including those used in nuclear power plant safety applications. The aim of this work is to demonstrate the effectiveness of nickel-doped graphene films on stainless steel as hydrogen recombination catalysts.

2. Experimental

To develop advanced catalytic materials for application in PAR, sintered porous 304L stainless steel filters were selected as substrates. These filters, with a diameter of 28 mm, a thickness of 2.5 mm, and a pore size of approximately 50 μm, were chosen to optimize gas diffusion and maximize surface area.

The substrates were coated with graphene using a non-thermal plasma technique (Ten et al., 2020), achieving an approximate 2 % increase in mass. Cyclohexane (Aldrich) served as the carbon precursor; while a 60 kV arc discharge was maintained under a continuous nitrogen (N_2) flow between a 316L stainless steel electrode and the substrate surface, enabling uniform graphene deposition. After coating, the substrates were thoroughly rinsed with deionizer water and isopropyl alcohol to remove residual impurities, and subsequently, dried under controlled conditions to preserve the integrity of the graphene layer.

Nickel was then introduced as the catalytic doping at mass loadings of 0.25 %, 0.50 %, 1.0 %, and 2.0 % by precisely dispersing $NiCl_2{\cdot}6H_2O$ (Aldrich) onto the coated substrates. The nickel species were reduced and securely anchored via the Flash Joule Heating Method (De Micheli et al., 2025), a rapid thermal processing technique that ensures metal nanoparticle fixation without compromising the underlying graphene structure.

Comprehensive characterization of the catalytic materials was performed using multiple analytical techniques. Scanning Electron Microscopy (SEM) was conducted with a JEOL JSM-IT700HR microscope equipped with a Schottky emission source to obtain images illustrating sample morphology and nickel distribution across different doping concentrations. X-ray Diffraction (XRD) analysis was carried out on a Miniflex II diffractometer with Cu Kα radiation (λ = 0.15406 Å), scanning 2θ from 2° to 90° at 2°/min. Crystalline phases in both the sintered stainless steel substrates and the deposited coatings were identified by comparison with the ICDD Powder Diffraction File (PDF) database.

Raman spectroscopy measurements were acquired using a Horiba Scientific Macro Ram spectrometer with a 785 nm excitation laser. Ten spectral accumulations per sample were collected with 30 s exposure time each to optimize the signal-to-noise ratio while minimizing potential sample damage, providing insight into the structural quality and defect density of the graphene coatings.

Surface wettability was evaluated via contact angle measurements in accordance with ISO 15989/2004 using a KINO-SL150E goniometry. For statistical reliability, at least five specimens per catalytic material were measured, with ten readings per specimen, and average values calculated to characterize hydrophilicity.

BET surface area measurements were carried out using a Micromeritics ASAP 2020 Plus analyzer. Prior to analysis, samples were degassed under vacuum at 150 °C for 12 h to remove adsorbed moisture and contaminants. The specific surface area was determined via the Brunauer–Emmett–Teller (BET) method using nitrogen adsorption isotherms at 77 K.

Hydrogen removal performance was assessed in a custom-built test station. Precisely weighed catalysts were placed inside a pressurized reaction chamber, and hydrogen, oxygen, and nitrogen gases were introduced in predetermined stoichiometric ratios to simulate relevant operational conditions. The catalytic reaction was continuously monitored, with real-time data acquisition and process control managed by in-house developed software, enabling precise evaluation of hydrogen conversion efficiency under controlled experimental parameters.

3. Results and discussion

Fig. 1 shows SEM images of sintered 304L stainless steel substrates coated with graphene and doped with nickel.

For the samples with lower nickel contents (0.25 % and 0.5 %), the surface exhibits a cracked, clay-like morphology, which is characteristic of a predominance of graphene-based material. This structure suggests that at these lower doping levels, nickel is not sufficiently abundant to form discrete particles or clusters, and the graphene layer dominates the surface features.

As the nickel content increases to 1.0 % and 2.0 %, distinct particles with varying brightness become evident. The darker particles are likely attributed to nickel oxide (Ni_xO_y), while the brighter particles correspond to metallic nickel. This contrast in brightness indicates the coexistence of oxidized and metallic nickel phases, which may influence the redox behavior and overall catalytic performance. In SEM images, metallic nickel particles appear brighter due to higher electron reflection, while nickel oxide (Ni_xO_y) appears darker.

Importantly, the sample with 2.0 % nickel shows a relatively uniform distribution of these particles across the surface, suggesting an improved dispersion of catalytic species. Such homogeneity is critical for catalytic efficiency, as it ensures that a greater number of active sites are accessible to facilitate more uniform interaction with reactant molecules.

The observed morphological evolution with increasing nickel content highlights the interplay between the graphene coating and nickel species. While graphene provides a high-surface-area scaffold promoting electron transport and stability, nickel incorporation introduces active catalytic sites. Therefore, the enhanced dispersion and the presence of both metallic and oxidized nickel in the 2.0 % sample suggest a synergistic effect, potentially leading to superior catalytic activity in applications such as hydrogen recombination or other redox reactions.

Fig. 2 shows XRD patterns of sintered porous metal substrates made from 304L stainless steel coated with graphene and doped with nickel with pore sizes of 50 μm.

Peaks centered at approximately 23.1°, 25.4°, and 44.4° (Santos et al., 2020) are attributed to carbonaceous phases, consistent with the presence of graphitic or graphene-like materials deposited on the substrate surface. The broad (002) peak at ~ 25.4° is indicative of few-layer graphene with a turbostratic or disordered stacking structure, typical of plasma-deposited carbon coatings.

Diffraction features associated with nickel species appear as broad and low-intensity peaks relative to the carbon and steel signals, suggesting either a small crystallite size or a high degree of dispersion of nickel within the graphene-coated matrix. Metallic nickel phases are identified by reflections at 38°, 44°, and 52°, which match the reference pattern (JCPDS #89–7128). Partial overlap is observed with NiO reflections (JCPDS #75–0269) at 37° and 42°, indicating the coexistence of metallic and oxidized nickel species in the doped coatings. This observation is consistent with the SEM analysis and suggests that the

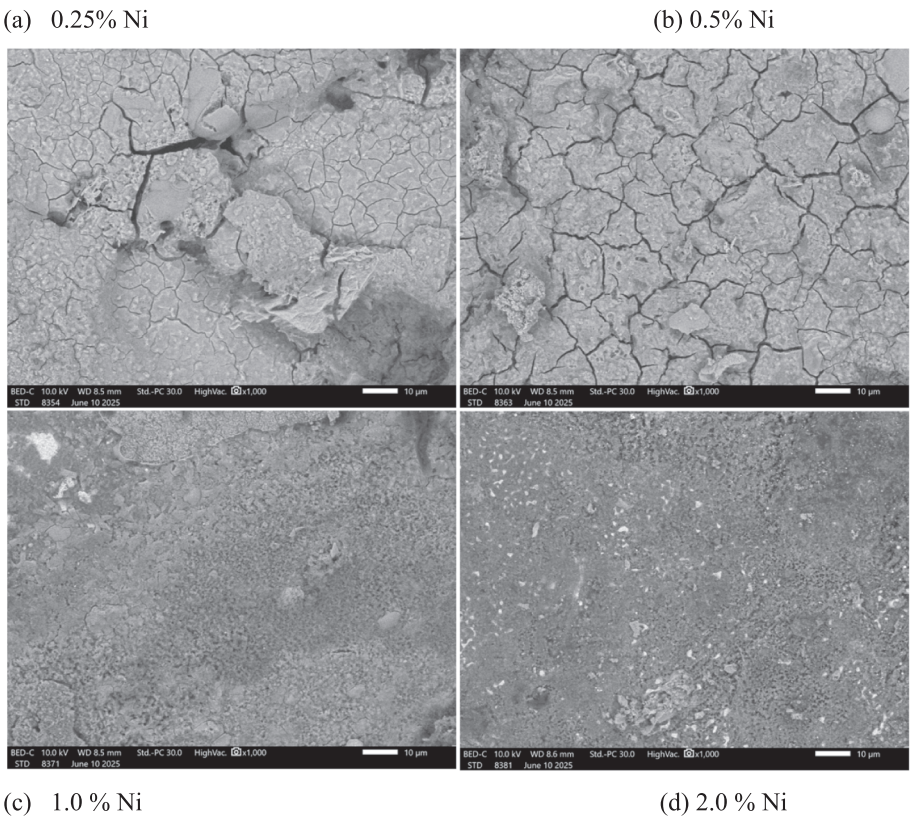

Fig. 1. SEM micrographs of sintered porous 304L stainless steel coated with graphene and doped with 0.25 (a), 0.50 (b), 1.0 (c) and 2.0 (d) % nickel on a substrate with pore sizes of 50 μm.

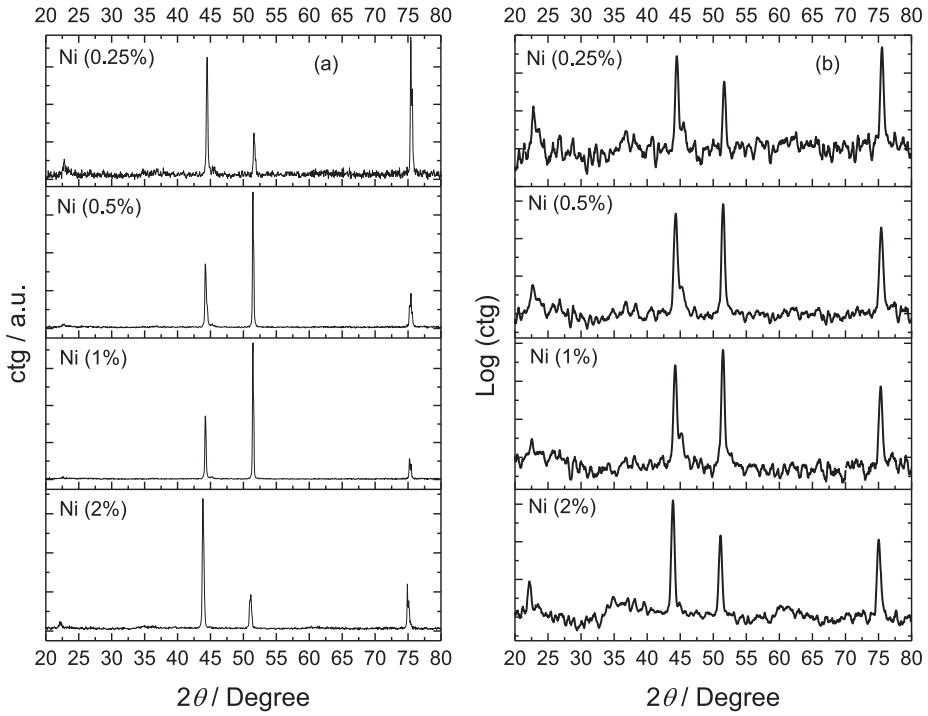

Fig. 2. XRD patterns of sintered porous metal substrates made from 304L stainless steel coated with graphene and doped with nickel (0.25 %,).5% 1.0 % and 2 %), with pore sizes of 50 μm. (a) A baseline correction was applied to all catalysts, and noise was removed from the measurements. and (b) raw XRD data.

Flash Joule Heating process promotes partial reduction of nickel ions, while some surface oxidation likely occurs upon exposure to ambient conditions. According to De Micheli et al. (De Micheli et al., 2025), the diffraction pattern of stainless steel typically exhibits reflections corresponding to austenite (~41.9°, 51.8°, and 75.4°) and martensite (44.3°, 65.1°, and 83°) phases, in addition to spinel-type oxides such as

$Mn_{1.5}Cr_{1.5}O_4$ and $FeCr_2O_4$, as well as Cr_2O_3, with characteristic peaks at approximately 16.7°, 30.3°, 35.8°, 56.7°, 61.5°, 71.9°, 72.3°, and 77.5°. These reflections are usually very intense and may overlap or mask the signals of other crystalline phases present in the coating, especially in samples with lower crystallinity or reduced nickel content, making the identification of Ni and NiO peaks less evident.

Fig. 3 presents the Raman spectra of the fabricated PAR materials. The experimental data are plotted as gray curves, while key spectral features are highlighted: the black lines indicate the main graphene-related bands D and G (~1320 and ~1595 cm^{-1}), the blue lines mark the D2, D3, and D4 bands, and features associated with nickel species are labeled in blue.

The first-order Raman spectra were deconvoluted using the five-band model (G, D2, D3 and D4) following the procedure proposed by De Micheli et al. (De Micheli et al., 2025).The prominent D band at ~1350 cm^{-1} is attributed to structural defects and lattice disorder in the sp^2 carbon network (De Micheli et al., 2025), typically arising from edges, vacancies, or sp^3-hybridized carbon. The G band at ~ 1580 cm^{-1} corresponds to the in-plane vibrational mode (E_2g symmetry) of sp^2-bonded carbon atoms, characteristic of graphitic materials (De Micheli et al., 2025). Additional broad featuresD2 (~1620 cm^{-1}), D3 (~1500 cm^{-1}), and D4 (~1235 cm^{-1}), overlapping with D)are commonly

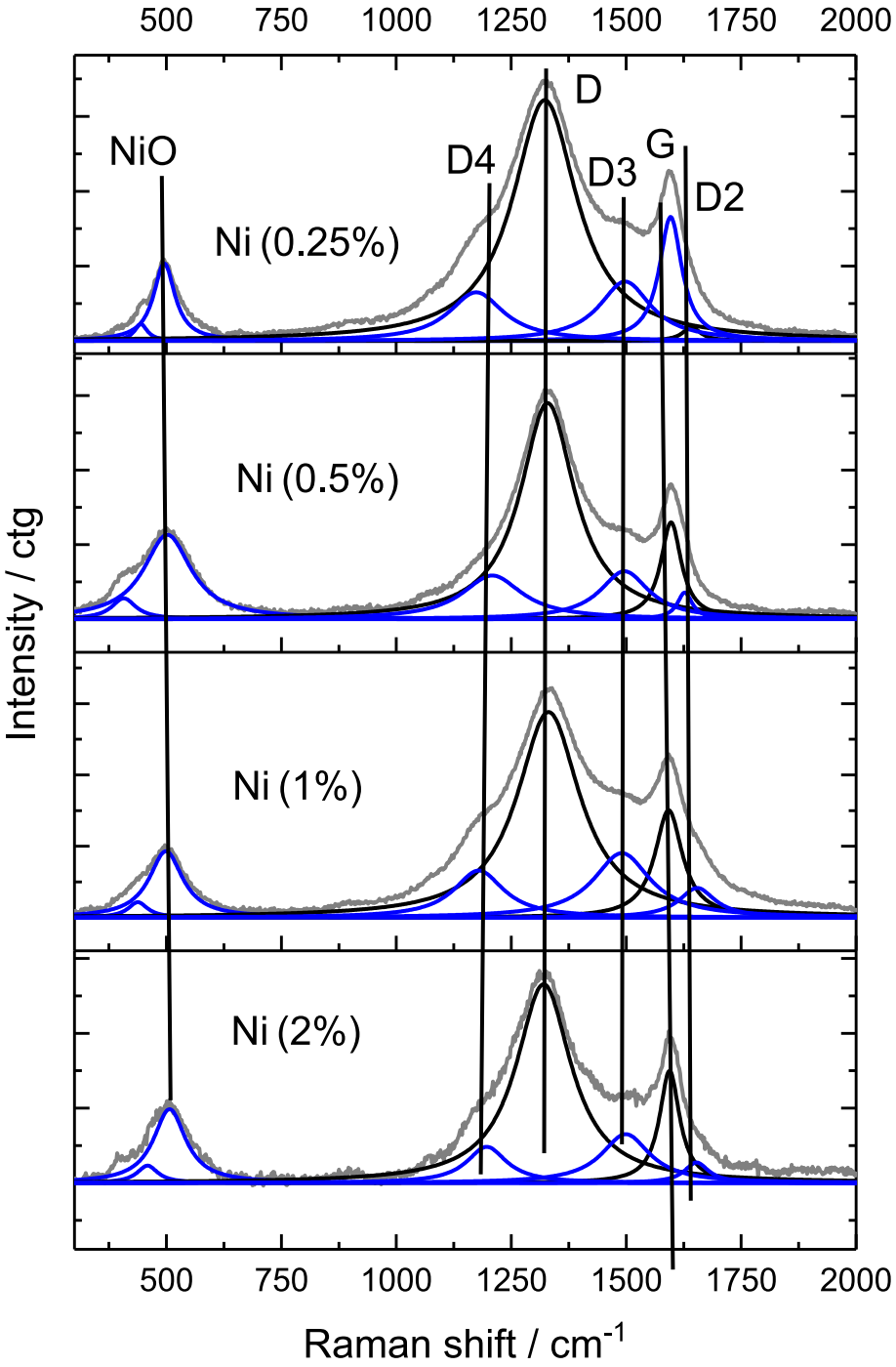

Fig. 3. Raman spectra of sintered porous metal substrates made from 304L stainless steel coated with graphene and doped with nickel 0.25, 0.5,1.0, and 2.0 wt% with pore size de 50 μm. The grey line represents the measured spectrum, the black line represents the principal bands (D, and G), the D2, D3 and D4 bands, and nickel bands are shown in blue.

associated with amorphous carbon, functional groups, or extended structural distortions beyond the pristine graphene lattice (De Micheli et al., 2025).

Analysis of the spectra reveals that increasing nickel loading influences the relative intensities of the D and G bands. The ID/IG ratio decreases from 5.79 (0.25 wt% Ni) to 5.42 (0.5 wt% Ni), 4.71 (1.0 wt% Ni), and 4.76 (2.0 wt% Ni), indicating a progressive reduction in defect density with higher nickel content. This trend suggests that elevated nickel concentrations promote structural ordering within the graphene layers, potentially due to metal-support interactions and strain-induced healing of defects during the Flash Joule Heating process. The incorporation of nickel oxide induce local healing, leading to partial defect passivation consistent with findings reported by Karoui et al. (Karoui et al., 2010).

Additionally, a distinct feature appears near 500 cm^{-1} in the nickel-doped samples, which is assigned to the longitudinal optical phonon mode of NiO, further confirming the presence of nickel oxide phases detected in XRD and SEM analyses. This observation reinforces the coexistence of metallic and oxidized nickel species on the graphene-coated surface, which may play a synergistic role in catalytic hydrogen recombination by facilitating redox cycling and hydrogen spill over.

Fig. 4 illustrates the hydrophobicity experiments for the catalysts prepared with 0.25, 0.50, 1.0, and 2.0 wt% of nickel.

The results indicate a gradual decrease in hydrophobicity with increasing nickel content. The 0.25 wt% Ni sample exhibited the highest contact angle (140°), characteristic of a strongly hydrophobic surface. Increasing the nickel loading to 0.50 wt% led to a contact angle of 124°, while further increases to 1.0 wt% and 2.0 wt% produced contact angles of 122° and 121°, respectively. This trend suggests that higher nickel contents may partially modify the surface morphology or mask hydrophobic regions of the grapheme coated support, potentially reducing the density of low-energy carbon surfaces available for water repellency.

Despite this slight decrease, all samples maintained contact angles above 120°, classifying them as strongly hydrophobic. This behavior aligns with previous reports by De Micheli (De Micheli et al., 2025; De Micheli et al., 2024), where graphene incorporation on porous 304L stainless steel increased the water contact angle from 38.1° (bare substrate) to 128°, highlighting the significant role of graphene in imparting hydrophobic character. The presence of armchair-type edges and well-ordered sp^2 carbon networks in the graphene layers likely contributes to this high water repellency.

The modest reduction in contact angle with increased nickel content can be attributed to several factors. First, nickel particles may introduce localized polar sites that slightly enhance water adsorption. Second, the deposition of nickel could create minor disruptions in the graphene lattice (sp^3-type defects), decreasing the overall hydrophobicity. Similar effects have been observed upon platinum doping, where water contact angles decreased due to the combination of metal carbon interactions and the introduction of lattice defects.

Overall, the hydrophobicity analysis demonstrates that while nickel incorporation slightly modulates surface wettability, the graphene-coated stainless steel substrates retain strong hydrophobic character. This property is advantageous for catalytic applications in gas-phase reactions, such as hydrogen recombination, because it promotes gas diffusion, minimizes water adsorption, and maintains the accessibility of active catalytic sites. Furthermore, the interplay between nickel loading and surface hydrophobicity may influence catalyst–reactant interactions, suggesting that optimization of metal content is crucial for balancing catalytic activity and surface properties.

BET surface area analysis revealed a significant evolution in the specific surface area of the catalysts with varying nickel content. The bare 304L stainless steel substrate exhibited a very low surface area (0.0036 m^2/g), typical of dense metallic alloys. Following graphene coating and nickel doping, a marked increase in surface area was observed: 0.25 wt% Ni (0.2135 m^2/g); 0.5 wt% Ni (5.2847 m^2/g); 1 wt% Ni (0.7597 m^2/g); and 2 wt% Ni (0.6509 m^2/g). Notably, the highest surface area was achieved at 0.5 wt% Ni—approximately 25 times greater than that of the other Ni-doped samples suggesting, in agreement with SEM micrographs, a highly porous and well-dispersed morphology at this composition, which enhances accessibility to catalytic sites. At higher Ni loadings, the surface area decreased, likely due to the formation of metallic Ni particles or aggregates, as confirmed by SEM and XRD, which hinder effective exposure of the graphene support and active sites.

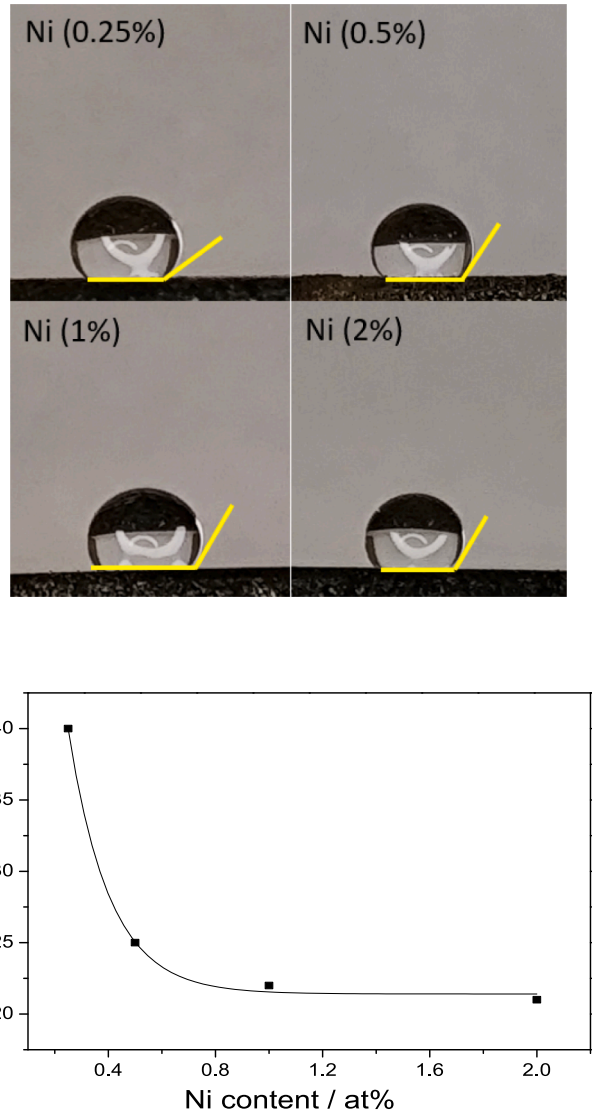

Fig. 4. Water contact angles of samples with 0.25, 0.5, 1.0, and 2.0 wt% Ni supported on porous 304L stainless steel coated with graphene (pore size: 50 μm). Contact angles were measured following ISO 15989/2004 using a KINO-SL150E goniometer. For each catalytic material, at least five specimens were tested, with ten measurements per specimen, and average values were used to characterize surface hydrophilicity. The data were then used to construct a plot relating hydrophobicity to nickel content.

These findings are consistent with the observed morphological evolution: at low Ni contents, a cracked surface morphology and dominant graphene coverage maximize surface exposure and reactant accessibility. In contrast, increased Ni agglomeration at 1.0 and 2.0 wt% leads to reduced surface area and possible saturation of active sites, aligning with the catalytic performance trends—peak efficiency was observed for 1.0 wt% Ni, with no further improvement at 2 wt%. Additionally, the degree of metallic coverage directly influences hydrophobicity; higher

Ni loading reduces the exposed graphene surface area, resulting in a slight decrease in the measured water contact angle.

Thus, the interplay between surface area and structural morphology is a key determinant of catalytic performance, highlighting that precise optimization of the nickel content is essential to maximize the efficiency of hydrogen recombines and to ensure the practical viability of this material in nuclear and energy-related applications.

Hydrogen recombination experiments were conducted using a custom-built test station developed in our laboratory. Catalysts containing 0.25, 0.50, 1.0, and 2.0 wt% nickel, supported on porous 304L stainless steel substrates coated with graphene (with a pore size of 50 μm), were placed inside a pressurized chamber under an inert nitrogen atmosphere to ensure controlled conditions. Following chamber purging, a controlled mixture of hydrogen and oxygen gases was introduced to simulate reactive environments. Real-time data acquisition was facilitated through a dedicated computational program, enabling precise monitoring of reaction parameters.

The results obtained from these experiments are illustrated in Fig. 5, demonstrating the performance of the catalysts under the specified conditions.

Fig. 5 presents the hydrogen recombination performance of graphene-coated porous 304L stainless steel substrates doped with varying nickel contents (0.25, 0.50, 1.0, and 2.0 wt%). The results demonstrate a clear dependence of catalytic activity on nickel loading. As it can be seen in Fig. 5a, after a strong decrease in the amount of hydrogen removal in the first minutes of the test, then the amount of hydrogen removal slightly decreases with time and after 60 min a nearly constant value is reached. The results demonstrate a clear dependence of catalytic activity on nickel loading for Ni $\leq$ 1.0 wt%, Above 1.0 wt% Ni, the amount of hydrogen removal is constant.

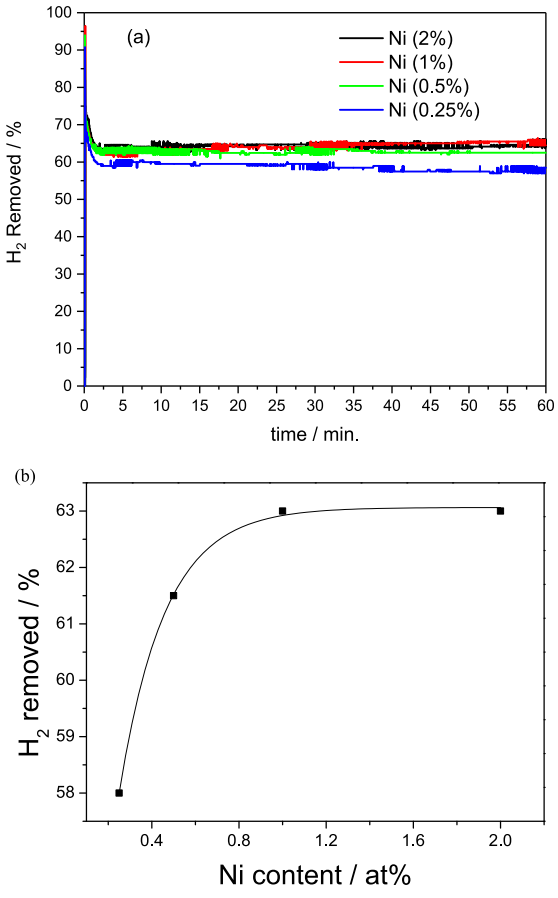

Fig. 5. Dependence of hydrogen removal in sintered porous metal substrates made from 304L stainless steel coated with graphene and doped with 0.25 Ni, 0.50 Ni, 1.0 Ni and 2.0 Ni% on (A) time and (B) Ni content.

The catalyst with the lowest nickel content (0.25 wt%) exhibited the lowest hydrogen removal efficiency, suggesting that the number of available active sites was insufficient to effectively promote hydrogen recombination. As the nickel content increased to 0.50, 1.0, and 2.0 wt %, a progressive improvement in hydrogen removal efficiency was observed, indicating a positive correlation between nickel loading and catalytic performance. This trend can be attributed to the greater availability of active metallic sites at higher Ni concentrations, which facilitates the recombination of hydrogen and oxygen molecules. For Ni $>$ 1.0 wt%, the amount of hydrogen removal no longer increases, due to the saturation of the positive effect of Ni doping, such as enhanced Ni-graphene interactions or creation of new active sites.

The graphene coating on the porous 304L substrate plays a crucial role in enhancing catalytic performance. It contributes to the uniform dispersion and stabilization of nickel particles, provides additional electrical conductivity, and imparts hydrophobicity, all of which are beneficial for gas–solid interactions and overall catalyst stability. Moreover, the porous structure with 50 μm pore size ensures efficient gas diffusion, promoting effective contact between hydrogen molecules and active sites on the catalyst surface.

Comparatively, De Micheli (De Micheli et al., 2025) reported that a 0.50 wt% platinum-doped porous stainless steel substrate (5.0 μm pore size) achieved a hydrogen removal efficiency of 39.9 % under similar conditions, more than five times higher than the 0.25 wt% platinum-doped sample. In this study, nickel based catalysts achieved approximately 63 % hydrogen removal at only 1.0 wt% Ni, demonstrating superior performance. It is important to note that Micheli's experiments were conducted in a reactor coupled with a residual gas mass analyzer, whereas the tests of this paper were performed in a controlled static test station. Despite these methodological differences, the results highlight the effectiveness of nickel as a more abundant and cost-efficient alternative to platinum, reinforcing the potential of Ni/graphene/304L stainless steel composites for practical hydrogen recombination applications.

Peng et al. (Peng et al., 2022) demonstrated that nanoporous Ni/NiO catalysts prepared via partial electro-oxidation after dealloying exhibit enhanced hydrogen evolution reaction (HER) activity, attributed to their high surface area, abundant active sites, and favorable electron transport pathways. The creation of nanopores effectively increases the electrochemically active surface area, facilitating more efficient adsorption and desorption of hydrogen intermediates, which is crucial for improving HER kinetics.

Zhang et al. (Zhang et al., 2024) reported that NiO/$NiCo_2O_4$ porous nanowires promote enhanced electrocatalytic glucose oxidation accompanied by hydrogen production. This improvement is largely due to interfacial synergistic effects between NiO and $NiCo_2O_4$, which facilitate charge transfer and improve catalytic selectivity. The study emphasizes that combining different transition metal oxides can effectively modulate electronic structures and reaction pathways, enhancing overall electrocatalytic performance.

Zhang et al. (Zhang et al., 2024) demonstrated that a Ni foam-supported Pt-Pd catalyst, designed for use in a passive catalytic recombiner for hydrogen, exhibited a maximum conversion of 51.96 % at a hydrogen concentration of 4 % and a flow velocity of 0.05 m/s. The Ni foam-supported Pt-Pd catalysts were prepared using two different methods: pine needle-like Pt-Pdnanodendrites were synthesized via the impregnation method, while Pt-Pdnanosheet catalysts were obtained through the electrodeposition method. The catalysts prepared by impregnation exhibited a catalytic activity 2.6 % higher than that ones prepared by electrodepositing. These results suggest that the catalytic performance strongly depends on the preparation method employed.

Lee (Do and Lee, 2023) explored hollow Ni/NiO/C composites derived from metal-organic frameworks (MOFs), which exhibited remarkable HER efficiency. The hollow architecture not only provides a high surface-to-volume ratio but also enables better mass transport and

mitigates aggregation of active sites, resulting in improved catalytic stability and long-term durability. These studies underline the importance of structural design, surface engineering, and interfacial effects in optimizing Ni/NiO-based catalysts. The combination of nanoporous architectures, synergistic bimetallic/oxide interfaces, and carbonaceous supports provides a multifaceted strategy to enhance electrocatalytic activity. These findings support the rationale for incorporating Ni/NiO nanostructures into advanced electrochemical devices, highlighting their potential in energy conversion and hydrogen generation applications.

Overall, the hydrogen recombination data confirm that the synergy between well-dispersed nickel nanoparticles, the graphene support, and the porous stainless steel substrate is critical for achieving high catalytic efficiency, while also offering an economically viable route for large-scale applications.

4. Conclusion

This study reports the design and development of a catalyst for PAR systems based on porous sintered AISI 304L stainless steel coated with graphene and doped with nickel nanoparticles. Morphological, structural, surface, and catalytic characterizations demonstrate that the combination of graphene with well-dispersed nickel species enables efficient hydrogen recombination under simulated accident conditions. The 304L stainless steel substrate provides mechanical stability, thermal resistance, and effective heat dissipation, while the graphene with nickel deposited, promotes hydrogen adsorption, and maintains strong hydrophobicity, supporting catalytic activity in humid environments. Nickel doping introduces active sites, with optimal performance observed at 1.0 wt% Ni, beyond which additional loading does not significantly improve activity, suggesting saturation of accessible catalytic sites.

SEM, XRD, and Raman analyses confirm successful deposition of few-layer graphene and the presence of both metallic nickel and nickel oxide phases, whose coexistence may facilitate redox cycles and hydrogen spill over during recombination. The decrease in the ID/IG ratio with increasing nickel content indicates a defect-modifying effect, likely due to metal–support interactions. Contact angle measurements show that all samples maintain high hydrophobicity ($\theta > 120^{\circ}$), favoring gas diffusion and minimizing water inhibition. Catalytic tests reveal a clear dependence of hydrogen conversion efficiency on nickel loading, with the 1.0 wt% Ni sample achieving the highest activity, comparable to noble-metal-based systems under similar conditions.

The use of nickel, an abundant and low-cost transition metal, together with scalable fabrication methods such as non-thermal plasma graphene deposition and Flash Joule Heating, provides a practical and economically viable alternative to conventional noble-metal-based PAR catalysts.

For future work, we plan to perform additional surface and compositional analyses, including X-ray photoelectron spectroscopy (XPS) and transmission electron microscopy (TEM), to gain deeper insight into the chemical state, dispersion, and nanoscale structure of the nickel species, further supporting the understanding and optimization of catalytic performance.

Overall, the results demonstrate that nickel-doped graphene-coated stainless steel substrates are a promising, cost-effective approach for hydrogen recombination applications, providing a feasible alternative to platinum-based systems in safety and hydrogen-energy infrastructures.

CRediT authorship contribution statement

L.M. Rios: Investigation. **L.De Micheli:** Formal analysis. **G. Silvestrin:** Methodology. **M. Durazzo:** Visualization. **E.F. Urano de Carvalho:** Visualization. **R.F.B. de Souza:** Writing – original draft. **C. Giovedi:** Writing – original draft, Supervision. **E. Antolini:** Writing – review & editing. **A.Oliveira Neto:** Writing – review & editing.

Declaration of competing interest

The authors declare that they have no known competing financial interests or personal relationships that could have appeared to influence the work reported in this paper.

Acknowledgments

We are grateful to CAPES, CNPq (350514/2023-2, 302820/2024-8), and FDTE for financial supports. Rodrigo Fernando Brambilla de Souza extends special gratitude to the execution team for the Brazilian Multipurpose Reactor (RMB/CNEN) Project.

Data availability

No data was used for the research described in the article.

References

Santos, L.L., Cardoso, R.P., Brunatto, S.F., 2020. Direct correlation between martensitic transformation and incubation-acceleration transition in solution-treated AISI 304 austenitic stainless steel cavitation. Wear 462–463, 203522. https://doi.org/10.1016/j.wear.2020.203522.

Karimi, N., Riffard, F., Rabaste, F., Perrier, S., Cueff, R., Issartel, C., Buscail, H., 2008. Characterization of the oxides formed at 1000°C on the AISI 304 stainless steel by X-ray diffraction and infrared spectroscopy. Appl. Surf. Sci. 254 (7), 2292–2299. https://doi.org/10.1016/j.apsusc.2007.09.018.

Malakhov, A.A., Avdeenkov, A.V., Bessarabov, D.G., 2024. Numerical and experimental analysis of cylindrical-type PAR catalyst behavior. Nucl. Eng. Des. 417, 112822. https://doi.org/10.1016/j.nucengdes.2023.112822.

Lee, S.-M., Lee, S.-H., Roh, J.-S., 2021. Analysis of activation process of carbon black based on structural parameters obtained by XRD analysis. Crystals 11 (2), 153. https://doi.org/10.3390/cryst11020153.

Shen, S.Y., Zhao, T.S., Xu, J.B., Li, Y.S., 2010. Synthesis of PdNi catalysts for the oxidation of ethanol in alkaline direct ethanol fuel cells. J. Power Sources 195 (4), 1001–1006. https://doi.org/10.1016/j.jpowsour.2009.08.079.

Simões, M., Baranton, S., Coutanceau, C., 2010. Electro-oxidation of glycerol at Pd based nano-catalysts for an application in alkaline fuel cells for chemicals and energy cogeneration. Appl Catal B 93 (3–4), 354–362. https://doi.org/10.1016/j.apcatb.2009.10.008.

Lu, Z., Wang, C., Chen, X., Song, M., Xia, W., 2021. Effects of buffer gas on N-doped graphene in a non-thermal plasma process. Diam. Relat. Mater. 118, 108548. https://doi.org/10.1016/j.diamond.2021.108548.

Wu, J.-B., Lin, M.-L., Cong, X., Liu, H.-N., Tan, P.-H., 2018. Raman spectroscopy of graphene-based materials and its applications in related devices. Chem. Soc. Rev. 47 (5), 1822–1873. https://doi.org/10.1039/C6CS00915H.

Ferrari, A.C., Basko, D.M., 2013. Raman spectroscopy as a versatile tool for studying the properties of graphene. Nat. Nanotechnol. 8 (4), 235–246. https://doi.org/10.1038/nnano.2013.46.

Day, C.S., Day, V.W., Shaver, A., Clark, H.C., 1981. Variations in platinum-carbon(sp3) bond lengths. Crystal and molecular structure of (1,5-cyclooctadiene)(η1-cyclopentadienyl)methylplatinum(II), Pt(1,5-C8H12)(η1-C5H5)(CH3). Inorg. Chem. 20 (7), 2188–2193. https://doi.org/10.1021/ic50221a049.

Malard, L.M., Pimenta, M.A., Dresselhaus, G., Dresselhaus, M.S., 2009. Raman spectroscopy in graphene. Phys. Rep. 473 (5–6), 51–87. https://doi.org/10.1016/j.physrep.2009.02.003.

Koyakutty, H., Niranjana, J.S., Bushiri, M.J., 2023. Defect rich Ni/NiO-grapheneheterostructures with oxygen bridges for enhanced electrocatalytic glucose oxidation towards selective sensing. Mater. Chem. Phys. 309, 128330. https://doi.org/10.1016/j.matchemphys.2023.128330.

Ten, G., Gerasimenko, A.Y., Savelyev, M.S., Kuksin, A.V., Vasilevsky, P.N., Kitsyuk, E.P., Baranov, V.I., 2020. Influence of edge defects on Raman spectra of graphene. J. Lett. Mater. 10, 89–93.

De Micheli, L., Silvestrin, G., de Souza, R.F.B., Oliveira Neto, A., Giovedi, C., 2025. Development of a porous 304L Stainless steel substrate enhanced with graphene and platinum for hydrogen mitigation in passive autocatalytic recombiners. Int. J. Electrochem. Sci. 20, 101128.

Karoui, S., Amara, H., Bichara, C., Ducastelle, F., 2010. Nickel-assisted healing of defective graphene. ACS Nano 4, 6114–6120. https://doi.org/10.1021/nn101822s.

De Micheli, L., Giovedi, C., Abe, A., Oliveira Neto, A., 2024. Nuclear power plants: recent advances towards to safety. Brazil. J. Radiat. Sci. 12, e2612.

Sanap, K.K., Varma, S., Waghmode, S.B., Bharadwaj, S.R., 2015. Wire gauze and cordierite supported noble metal catalysts for passive autocatalytic recombiner. Nucl. Eng. Des. 294, 226–232. https://doi.org/10.1016/j.nucengdes.2015.09.010.

Kozhukhova, A.E., duPreez, S.P., Malakhov, A.A., Bessarabov, D.G., 2021. A thermally conductive Pt/AAO catalyst for hydrogen passive autocatalytic recombination. Catalysts 11, 491. https://doi.org/10.3390/catal11040491.

Kozhukhova, A.E., du Preez, S.P., Bessarabov, D.G., D.g., 2022. Preparation of Pt/Ce–Zr–Y mixed oxide/anodized aluminium oxide catalysts for hydrogen passive

autocatalytic recombination. Int. J. Hydrogen Energy 47, 12726–12738. https://doi.org/10.1016/j.ijhydene.2022.01.246.

Musavuli, K.C., Malakhov,A., Everson, R.C., Kozhukhova, A., Modisha, P., Bessarabov, D. (2024). Passive autocatalytic recombination of hydrogen on a Pt/Al_2O_3-coated metal foam: Experimental evaluation and CFD modelling, Int. J. Hydrogen Energy,94, 1374-1388. Jushang Zhang, Qihui Zhao, Tianming Man, Yunhe Zhao, ZehuaGuo, Ming Ding. Nucl. Eng. Design. 443, November 2025, 114355.

Peng, L., Liang, Y., Wu, S., Li, Z., Sun, H., Jiang, H., Zhu, S., Cui, Z., Li, L., 2022. Nanoporous Ni/NiO catalyst for efficient hydrogen evolution reaction prepared by partial electro-oxidation after dealloying. Appl. Surf. Sci. 592, 153313. https://doi.org/10.1016/j.apsusc.2022.153313.

Zhang, Z., Zhao, Q., Man, T., Zhao, Y., Guo, Z., Ding, M., 2024. Enhanced electrocatalytic glucose oxidation assisted hydrogen production via the interfacial synergistic effect of NiO/NiCoO porous nanowires. Green Chem. 26 (2), 452–460. https://doi.org/10.1039/d4gc01860e.

Do, H.H., Lee, J.H., 2023. Hollow Ni/NiO/C composite derived from metal-organic frameworks as efficient electrocatalysts for hydrogen evolution reaction. Nano Convergence 10 (1), 1–9. https://doi.org/10.1186/s40580-023-00354-w.